Polymer Chemistry

ROYAL SOCIETY OF CHEMISTRY

PAPER

View Article Online
View Journal

Cite this: DOI: 10.1039/d6py00149a

Direct end-group modification of poly(Aib)-polymers: heterogeneous peptide coupling and chiral folding

Sandipan Roy,[a] Christian Hildebrand,[a] Matthias Rohmer,[a] Yishen Xie,[b] Jitul Deka,[b] Justus F. Thümmler[a] and Wolfgang H. Binder *[a]

Helical poly(α-aminoisobutyric acid) is a foldamer capable of transmitting chiral information along achiral polymer-backbones. Yet its post-polymerization modifications after ring opening polymerization (ROP) remain challenging due to its poor solubility and limited reactivity. We here report a robust strategy for end-group functionalization of poly(Aib), obtained after ROP under heterogeneous conditions, enabling efficient coupling of a wide variety of end groups using stereochemically distinct initiators, such as point chiral amines, axially chiral binaphthols, and overcrowded alkene-based Feringa's photoswitches. The resulting polymers were post-functionalized *via* peptide-type coupling under varying conditions, employing different carboxylic acids and coupling agents in various solvents to introduce chemically distinct termini. MALDI-TOF mass spectrometry was used to assess purity and to monitor characteristic mass shifts associated with the respective end-group incorporation, thereby proving successful post-polymerization modification. Circular dichroism spectroscopy further confirmed transfer of chiral information from the initiators and the preservation of the helical secondary structure after functionalization. Among the tested polymers, the lipoic-acid-endgroups exhibited the highest coupling efficiency able to adsorb onto gold surfaces *via* disulfide–gold affinity, forming thin polymer films as evidenced by AFM and XPS analyses. The work establishes a versatile, heterogeneous post-functionalization strategy for tailoring helical poly(Aib) architectures with defined chiralities and surface-binding functionality, enabling the design of both static and dynamic chiral interfaces for next-generation molecular devices.

Received 13th February 2026,
Accepted 23rd May 2026

DOI: 10.1039/d6py00149a

rsc.li/polymers

Introduction

The synthesis of polypeptides enables the generation of precisely folded macromolecular structures, well-organised into 3D proteins, wherein the precise placement of monomers is crucial for arranging polymer segments into helices, beta-sheets, or beta-turns. Mainly concentrating on the 21 common amino acids, the proteinogenic building blocks are expanded by nature by a large number of amino acids, less well known, but present in many peptides.[1] Thus α-aminoisobutyric-acid (Aib) is a well-known amino acid in nature, found in peptaibols, bacterial peptides that induce permeabilisation of bacterial cell membranes.[2–6] Arranged as oligomers inside a peptide, they form a special type of helix, the 3_{10}-helix, stabilized by four consecutive intramolecular N···H···O═C H-bonds, which is different from the conventional alpha-helix generated from other amino acids.[7,8] The second important feature of the nonchiral amino-acid building block is its ability to fold into *P*- or *M*-helices, depending on one attached chiral unit at the chain-head of the oligomer[9] *via* the sergeant/soldier principle.[10] Thereby the screw-sense of the helix can be transponded, depending on the chirality of the covalently attached head group. There have been significant contributions regarding the ability to carry chiral information through the poly (Aib)-chain by Clayden,[11–14] reporting the ability to transfer chiral information through an oligomeric Aib-chain, also by use of photochemical switches.[12,13] Thus, also based on their exciting electronic effects, the peptides and polymer derived from Aib are attractive transporting systems of chiral information[15] over larger distances.[1,16–18] However, the length of such oligomers is limited by the often poor solubility of such poly(Aib)*n*-polymers with $n > 10$, required to bear defined end groups on both sides: the chiral head group to induce chirality and a defined end group to allow the proper positioning of the molecule, *e.g.* on a surface for use in a device, where chiral information is carried form the polymer's head group to the underlying chip.

[a]*Macromolecular Chemistry, Division of Technical and Macromolecular Chemistry, Faculty of Natural Sciences II (Chemistry, Physics, Mathematics), Institute of Chemistry, Martin Luther University Halle-Wittenberg, von-Danckelmann-Platz 4, D-06120 Halle, Germany. E-mail: wolfgang.binder@chemie.uni-halle.de*
[b]*Max Planck Institute for Microstructure Physics, Weinbergweg 1, D-06120 Halle (Saale), Germany*

Longer stretches of such polypeptides can either be prepared by solid-phase synthesis, as conventionally probed by biochemists, or *via* ring opening polymerization (ROP) of *N*-carboxyanhydrides.[19,20] We recently have prepared Aib-polymers by ring opening polymerization of Aib-*N*-carboxyanhydrides, using chiral amine initiators to elongate the chain length for chiral information transfer.[1,17,18] Although we succeeded in the use of amine-based initiators to effect a homogeneous polymerization of the respective *N*-carboxyanhydrides, control of the chain ends after polymerization remains complex.[16] One challenge in the polymerization and subsequent end group functionalization is the insolubility of the poly(Aib) polymer when exceeding more than ~8 units, so that all subsequent chemistry can only be accomplished under heterogeneous conditions. Although solid state polymerization of Aib-NCAs leads to a longer chain length,[17] the quest to effect an efficient end group-chemistry of those polymers remains unsolved.

Modification of poly(amino-acid) polymers and oligomers after ring-opening polymerization of NCAs has been largely accomplished in the side-chain of the respective NCA monomers or *via* the initiating unit.[21–23] Post-functionalization of terminal amino groups mainly focuses on direct chain extension by adding another NCA monomer to generate block-copolypeptides.[24] However, this is usually accomplished directly within the same polymerization by sequential monomer addition or by subsequent initiator-based introduction of functional groups enabling click-chemistry approaches.[25]

A direct modification of the terminal NH_2 group after ROP of such NCAs is, in the case of poly(Aib) oligomers, difficult to accomplish. Main challenge therein is the limited nucleophilicity and steric hindrance of the amino group due to two adjacent methyl groups and the limited solubility of the Aib oligomers. This represents a major challenge, as only suspension-based methods can be used for such modifications. Although poly(Aib) oligomers can be dissolved in fluorinated alcohols such as hexafluoroisopropanol, it fails in many nucleophilic substitution reactions.[26] We therefore sought to address the challenge of embedding a modification chemistry on both sides of an Aib-oligomer, using functional initiators acting as chiral inductors and non-chiral terminal agents, capable of binding the oligomers to an Au surface.

We here report a method to introduce appropriate end groups onto chiral Aib-polymers directly after ROP, so that the end group can be affixed, as checked by MALDI-TOF methods. We further introduce end groups which are nonchiral, to effect a stable binding of the poly(Aib) to surfaces without impeding the effect form the chiral-head group. The concept here is to introduce end groups that carry disulfide moieties, which can bind to Au surfaces in the sense of a self-assembled polymer layer (SAM) to study the resulting chiral induced spin selective effect (CISS).[30] We therefore chose different types of initiators (point-chiral, axial-chiral, photoswitchable) to transfer chirality to the poly(Aib)-chain and further probe various chemistries to introduce end groups *via* peptide-coupling directly after the polymerization, to exploit the potential of the residual NH_2 groups at the respective chain ends of the polymers. We discuss the various reaction conditions required to effectively transform the end group into the desired substituents, also highlighting the transfer of chiral information from the head-group. Data from different coupling methods under heterogeneous reaction conditions, as well as MALDI-TOF results, are reported here.

Experimental part

Materials

All chemicals were obtained from commercial suppliers and used without further purification unless otherwise noted. Chiral amine and binaphthol initiators, 2,5-dimethylanisole, polyphosphoric acid (PPA), thionyl chloride, titanium tetrachloride, methylmagnesium iodide, acetyl chloride, methacrylic acid and the resolving agent (8*S*,9*R*)-(−)-*N*-benzylcinchonidinium chloride were all purchased from Sigma-Aldrich. Lipoic acid, ferrocenecarboxylic acid and EDC hydrochloride were purchased from BLDpharm. PyBOP was obtained from Novabiochem, DIPEA from TCI, and DCC from Fluka. Boc-protected glycine and hexafluoroisopropanol (HFIP) were obtained from ABCR. Triphosgene and 2-aminoisobutyric acid were also purchased from ABCR. DMF and THF were purified using a solvent purification system (SPS). Hexane was dried over sodium and freshly distilled under a nitrogen atmosphere prior to use. Ethyl acetate was dried over P_2O_5. Deuterated chloroform ($CDCl_3$-d) and deuterated DMSO (DMSO-d6) were purchased from Chemotrade and deuterated 1,1,1,3,3,3-hexafluoro-2-propanol (HFIP-d2) was obtained from ARMAR.

Methods

Matrix-assisted laser desorption/ionization time-of-flight mass spectrometry (MALDI-TOF MS) was performed on a Bruker Autoflex III system (Bruker Daltonics) using a nitrogen laser operating at a wavelength of λ = 337 nm in positive reflection mode. Dithranol was used as the matrix (c = 20 mg mL^{-1} in THF) and NaTFA (c = 20 mg mL^{-1} in THF) as the salt. The analyte was prepared as a 20 mg mL^{-1} solution in DMF. The used matrix : analyte : salt ratio was 100 : 10 : 1, and 1 μL of the mixture was spotted on the MALDI target. Data evaluation was conducted using the flexAnalysis software (version 3.4), and simulation of the isotopic pattern was performed with Data Analysis software (version 4.0).

CD spectroscopy was conducted using JASCO J-1500 equipped with a PTC-510 cell holder. Polymer solutions were prepared in HFIP by diluting a 4 mg mL^{-1} stock to a final concentration of 0.02 mg mL^{-1}. Spectra were recorded over the wavelength range of 185–260 nm (and up to 400 nm where applicable) at a scanning speed of 100 nm min^{-1} with 20 accumulations. Baseline subtraction of the solvent was performed to obtain the corrected spectra. Data analysis was performed using Spectra Analysis Software.

Gel permeation chromatography (GPC) was conducted using 1,1,1,3,3,3-hexafluroisopropan-2-ol as solvent. HFIP-based SEC measurements with 0.1 mol l^{-1} KTFAc were per-

formed at 35.0 °C on a Viscotek GPCmax VE 2001 from Malvern by applying a PSS PFG precolumn and a PSS PFG main column. Sample concentration was adjusted to 3 mg mL^{-1} while applying a flow rate of 1 mL min^{-1}. Refractive index detection was performed using a VE 3580 RI detector from Viscotek. For determination of the molecular weights, external calibration was used *via* polymethyl methacrylate (PMMA) standards (purchased from PSS) with molecular weights ranging from 602 to 62.200 g mol^{-1}. OmniSEC software (version 5.12.).

X-ray photoelectron spectroscopy (XPS) was conducted on a K-Alpha+ Surface Analysis from Thermo Fischer Scientific using the Thermo Avantage software version 5.9925. The measured spot size was 400 µm with an energy step size of 0.1 eV and a pass energy of 50 eV. The dwell time for the measurement was 50 seconds, and each measurement consists of 10 scans. The obtained data were then displayed in Origin software.

Atomic force microscopy (AFM) was performed using a Nanosurf CoreAFM with Tap190AI-G cantilevers in the phase-contrast mode. The vibrational amplitude was set to 1 V. As parameters, a P-Gain of 1500, an I-Gain of 1000, and a D-Gain of 0 were used, with a time per line of 1 second. Data analysis was done using Gwyddion 2.53.

NMR spectroscopy was performed on either a 400 MHz, 600 MHz or 800 MHz Agilent Technologies VNMRS series spectrometer. Deuterated solvents were purchased from ARMAR. Proton and carbon NMR spectra were referenced using residual solvent signals. For interpretation of NMR-data Mestrenova software (version 16.0) was used.

Results and discussion

Synthesis of Aib-polymers

First, the Aib-NCA monomer was prepared from Aib following the method described in our earlier work.[27] The monomer was obtained in a 66% yield, and its purity was confirmed using ^{1}H and APT NMR spectroscopy (see SI 3 and 4). Polymerization of the monomer was conducted *via* solution ROP at 80 °C in DMF (see Fig. 1) using a diverse set of chiral amine and alcohol initiators. The initiators comprised three stereochemically distinct classes: point-chiral (*R*)- and (*S*)-1,2,3,4-tetrahydronaphthlene-1-amine (A*); axially chiral (*R*) and (*S*)-1,1′-bi-2-naphthol (B*); and the Feringa-type overcrowded alkene-photoswitch initiators (C*), specifically second-generation (6,6′-diol) framework—(2*R*,2′*R*,*Z*)-2,2′,4,4′,7,7′-hexamethyl-2,2′,3,3′-tetrahydro-[1,1′-biindenylidene]-6,6′-diol and its (2*S*,2′*S*,*Z*) enantiomer. The Feringa's photoswitches (C*) were prepared following a literature-reported three-step synthesis and a subsequent chiral resolution using *N*-benzylcinchonidinium chloride as the resolving agent.[28] Purity after each step was verified using ^{1}H- and ^{13}C-NMR spectroscopy, while the enantiopurity of the final compounds was confirmed by Circular Dichroism (CD) spectroscopy (see SI 5–14 and 54). These initiators were chosen to encompass a broad range of stereogenic environments, thereby enabling a systematic evaluation of how these chiral motifs influence induction through the otherwise achiral poly (Aib) backbone. The polymer, denoted as $\mathbf{A^R\text{-}P_0\text{-}E_0}$ (Table 1), was obtained using the $\mathbf{A^R}$ initiator and served as the parent material for the majority of the coupling reactions. MALDI-TOF MS was used as the primary method to determine

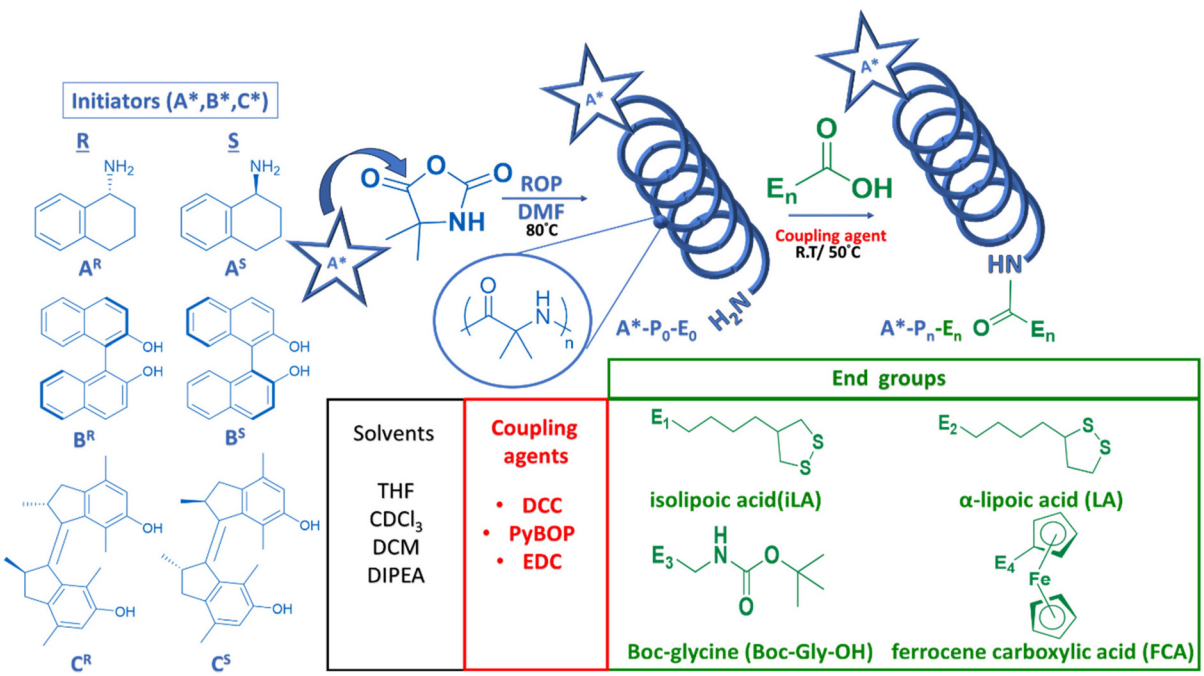

Fig. 1 Schematic overview of the ROP of Aib-NCA using chiral initiators and the subsequent end-group modifications with different functional acids.

Table 1 End-group modification of poly(Aib) chains derived from the unmodified parent polymers (**A***, **B***, **C***-P_0-E_0; both *R* and *S* enantiomers) under various coupling conditions using the free-amino group and carboxylic acids

Entry	Polymer	End group	Molar equivalents of acid	Solvent	Reaction time	Temp.	Coupling agent	Molar equivalents of coupling agent	Molar equivalents of base (DIPEA)	End-group modification [%] (analyzed by MALDI/*NMR)
1	$\mathbf{A}^{R}$-$\mathbf{P}_1$-$\mathbf{E}_3$	Boc-Gly-OH	3.5	THF	4 days	20 °C	DCC	3.5	—	53
2	$\mathbf{A}^{R}$-$\mathbf{P}_2$-$\mathbf{E}_3$	Boc-Gly-OH	3.6	THF	4 days	20 °C	PyBOP	3.5	3.0	60
3	$\mathbf{A}^{R}$-$\mathbf{P}_3$-$\mathbf{E}_3$	Boc-Gly-OH	2.7	DCM	4 days	20 °C	PyBOP	3.0	3.0	79
4	$\mathbf{A}^{R}$-$\mathbf{P}_4$-$\mathbf{E}_3$	Boc-Gly-OH	4.0	DCM	4 days	20 °C	EDC	4.0	10.0	92,*93
5	$\mathbf{A}^{S}$-$\mathbf{P}_5$-$\mathbf{E}_3$	Boc-Gly-OH	3.0	$CHCl_3$	1 day	50 °C	EDC	3.0	7.0	69
6	$\mathbf{A}^{R}$-$\mathbf{P}_6$-$\mathbf{E}_4$	FCA	1.1	THF	4 days	50 °C	PyBOP	2.4	6.0	*10
7	$\mathbf{A}^{S}$-$\mathbf{P}_7$-$\mathbf{E}_4$	FCA	4.0	THF	10 days	20 °C	PyBOP	4.0	6.0	*24
8	$\mathbf{A}^{R}$-$\mathbf{P}_8$-$\mathbf{E}_1$	iLA	1.0	THF	4 days	20 °C	PyBOP	1.2	3.0	62, *57
9	$\mathbf{A}^{S}$-$\mathbf{P}_9$-$\mathbf{E}_1$	iLA	1.0	THF	4 days	20 °C	PyBOP	1.2	3.0	64
10	$\mathbf{A}^{R}$-$\mathbf{P}_{10}$-$\mathbf{E}_2$	LA	2.0	THF	4 days	20 °C	PyBOP	2.4	6.0	85
11	$\mathbf{A}^{R}$-$\mathbf{P}_{11}$-$\mathbf{E}_2$	LA	2.0	THF	4 days	50 °C	PyBOP	2.4	6.0	97
12	$\mathbf{A}^{R}$-$\mathbf{P}_{12}$-$\mathbf{E}_2$	LA	4.0	THF	4 days	50 °C	PyBOP	4.8	12.0	96
13	$\mathbf{B}^{R}$-$\mathbf{P}_{13}$-$\mathbf{E}_1$	iLA	2.0	THF	4 days	20 °C	PyBOP	2.4	6.0	83
14	$\mathbf{B}^{S}$-$\mathbf{P}_{14}$-$\mathbf{E}_1$	iLA	2.0	THF	4 days	20 °C	PyBOP	2.4	6.0	83, *71
15	$\mathbf{C}^{R}$-$\mathbf{P}_{15}$-$\mathbf{E}_1$	iLA	2.0	THF	4 days	20 °C	PyBOP	2.4	6.0	82
16	$\mathbf{C}^{S}$-$\mathbf{P}_{16}$-$\mathbf{E}_1$	iLA	2.0	THF	4 days	20 °C	PyBOP	2.4	6.0	85

Polymer codes: A, B, and C denote the initiator class (A = chiral amine, B = axially chiral binaphthol, C = Feringa's photoswitch); superscript *R*/*S* indicates initiator chirality; the number *n* in P_n differentiates the polymer samples; E_n denotes the introduced end-group (E_1 = iLA, E_2 = LA, E_3 = Boc-Gly-OH, E_4 = FCA) (see Fig. 1). End-group conversion quantified by MALDI-TOF MS unless marked (*), where ^{1}H NMR was used, and values are reported as whole numbers rounded off to the nearest integer. Percentage conversion values are semi-quantitative and were calculated from the intensity ratio of the modified and unmodified peaks for the same degree of polymerization.

the chemical composition, chain length, and molecular weight of the polymers. As seen in Fig. 2a, the MALDI-TOF mass spectra of $\mathbf{A}^{R}$-$\mathbf{P}_0$-$\mathbf{E}_0$ exhibited a single, well-defined series of peaks consistent with polymers initiated *via* the Normal Amine Mechanism (NAM), incorporating the initiator at the chain terminus, displaying polymers bearing the chiral initiator on one end and the terminal $-NH_2$ group on the other end. The absence of any secondary peak distributions indicated that the Activated Monomer Mechanism (AMM) was effectively suppressed by conducting the polymerization under rigorously anhydrous conditions, using purified reagents and excluding catalytic impurities or adventitious acids known to promote the AMM.[18] The mass spectrum confirmed the formation of poly(Aib) with chain lengths ranging from 11 to 18 repeating units, with the most intense peak at m/z = 1360.922 representing 14 repeating units. Similar MALDI-TOF MS profiles were obtained for $\mathbf{B}^{R}$-$\mathbf{P}_0$-$\mathbf{E}_0$ and $\mathbf{C}^{S}$-$\mathbf{P}_0$-$\mathbf{E}_0$ (Fig. 3a and c), showing a well-resolved series of peaks corresponding to the respective initiator incorporated into the polymer chain terminus. Gel Permeation Chromatography (GPC) analysis of $\mathbf{A}^{R}$-$\mathbf{P}_0$-$\mathbf{E}_0$ and $\mathbf{B}^{R}$-$\mathbf{P}_0$-$\mathbf{E}_0$ in HFIP revealed a Polydispersity Index (PDI) of 1.27 and 1.30, respectively, indicating a relatively narrow molecular weight distribution (see SI 20 and 21).

End-group modification of poly(Aib) polymers

End-group modification of $\mathbf{A}^{R}$-$\mathbf{P}_0$-$\mathbf{E}_0$ was carried out starting from the terminal amine group, through a series of coupling reactions to incorporate the desired terminal moieties, expanding the versatility of the poly(Aib) architecture. To evaluate the efficiency of functionalization, a representative set of carboxylic acids – isolipoic acid (iLA, E_1), its chiral analogue α-lipoic acid (LA, E_2), Boc-glycine (Boc-Gly-OH, E_3), and ferrocene carboxylic acid (FCA, E_4) – were coupled to the polymer chain terminus using various coupling agents (EDC, DCC, PyBOP) in different solvents and temperature conditions. The selected end groups were chosen for distinct functional roles: LA (E_1) and iLA (E_2) possess a disulfide-containing dithiolane ring, enabling strong chemisorption onto gold surfaces for the preparation of a self-assembled polymer layer. Boc-Gly-OH (E_3) and FCA (E_4) were selected due to their potential utility as molecular probes for future investigations of chirality transfer along the polymer backbone, with glycine offering a simple chiral recognition handle after deprotection and ferrocene serving as a redox-active, spectroscopically traceable chiral reporter. Post-functionalization of the polymer was carried out by coupling the terminal amine with selected carboxylic acids under peptide-type coupling conditions. In a typical procedure, the selected carboxylic acid and the coupling agent were first combined in flame-dried glassware and subjected to several vacuum/nitrogen cycles. The solvent was added, following the base to activate the carboxylic acid. The mixture was stirred for 15 minutes, after which the parent poly(Aib) polymer was added. The solution was stirred for several days at room temperature or elevated temperature to

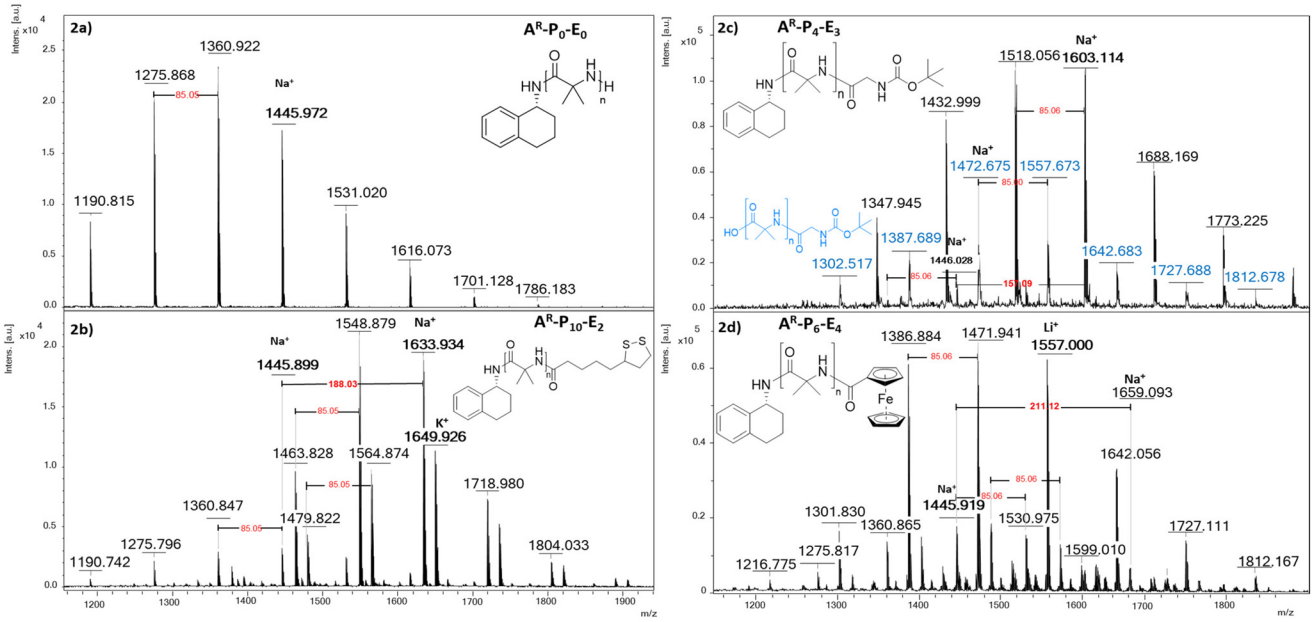

Fig. 2 MALDI-TOF MS spectra of poly(Aib) chains: (a) parent chain A^R-P_0-E_0, (b) lipoic acid (LA) functionalized A^R-P_{10}-E_2, (c) Boc-glycine (Boc-Gly-OH) functionalized A^R-P_4-E_3, and (d) ferrocene carboxylic acid (FCA) functionalized A^R-P_6-E_4.

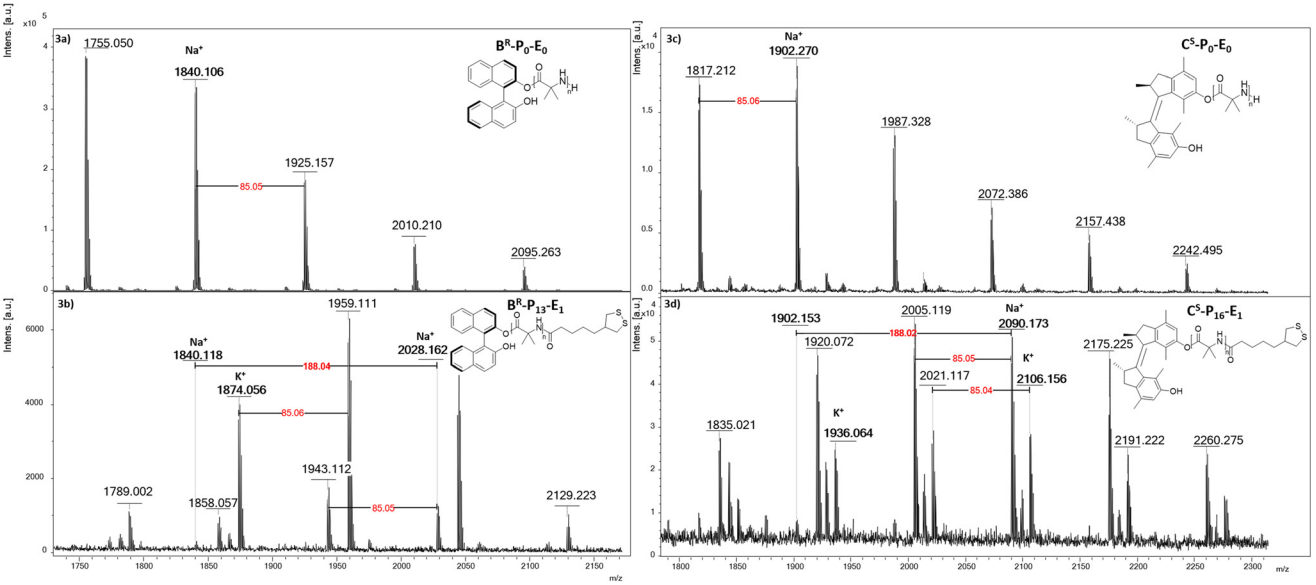

Fig. 3 MALDI TOF MS spectra of poly(Aib) chains: (a) parent chain B^R-P_0-E_0, (b) isolipoic acid (iLA) functionalized B^R-P_{13}-E_1, (c) parent chain C^S-P_0-E_0, and (d) isolipoic acid (iLA) functionalized C^S-P_{16}-E_1.

ensure adequate conversion. As the polymer was insoluble in all tested solvents, the modifications were carried out under heterogeneous conditions, with functionalization occurring at the polymer–solvent interface. Reaction time and the molar equivalents of reagents were varied to optimise the coupling efficiency.

Evaluation of end-group functionalization using MALDI-TOF MS spectroscopy

All polymers were analysed using MALDI-TOF mass spectroscopy to evaluate end-group incorporation following post-polymerisation coupling reactions (see Fig. 2 and 3(a–d)).

MALDI-TOF MS is not inherently quantitative, as ionisation efficiencies can vary between species, resulting in intensity differences that do not accurately reflect molar ratios. To render the analysis semi-quantitative, we applied a sensitivity (physical mixture) approach previously reported for MALDI calibration.[29,30] Following this methodology, we measured sensitivity plots by quantifying the intensity of defined physical mixtures in the MALDI spectra, while maintaining constant instrumental parameters, such as laser power, acceleration voltage, and spot size. For this purpose, we selected $\mathbf{A}^{R}$-$\mathbf{P_{11}}$-$\mathbf{E_2}$, which showed one of the highest ratios between modified and unmodified chains, and prepared mixtures of modified and unmodified polymers at defined weight ratios (W_{mod}/W_{unmod} = 0.11–9.0). The intensity ratio of the modified to the unmodified peak at the same degree of polymerization (DP = 15) was then plotted against the weight ratio, yielding a linear correlation ($R^2 \approx 0.992$, $r \approx 0.996$; see SI 22 and 23), so generating a sound basis for a (semi)-quantitative assessment of the endgroup-transformation efficiency. On this basis, end-group conversions for the broader sample set were estimated semi-quantitatively from MALDI spectra by comparing the relative intensities of modified and unmodified chains of the same DP, assuming similar ionization behavior across this series of structurally related polymers sharing an identical backbone. To further support this approach, we compared the conversion values obtained from MALDI-based estimates with those from ^{1}H-NMR spectroscopy for three representative systems with distinct end groups (Boc-Gly-OH and iLA). The values were in agreement and within the same range ($\mathbf{A}^{R}$-$\mathbf{P_4}$-$\mathbf{E_3}$: 92% *vs.* 93%; $\mathbf{A}^{R}$-$\mathbf{P_8}$-$\mathbf{E_1}$: 62% *vs.* 57%; $\mathbf{B}^{S}$-$\mathbf{P_{14}}$-$\mathbf{E_1}$: 83% *vs.* 70.5%; see SI 15–17), indicating that MALDI-derived conversions are consistent with independent NMR analyses, where applicable. In cases of selective ionisation, such as the ferrocene-functionalized samples (FCA), quantification was performed using ^{1}H-NMR spectroscopy. A detailed summary of the experimental parameters and the corresponding degrees of end-group conversions is provided in Table 1. For Boc-Gly-OH, moderate to high degrees of end-group conversion were obtained (53–92%) depending on the coupling system. $\mathbf{A}^{R}$-$\mathbf{P_1}$-$\mathbf{E_3}$ (entry 1), synthesized using DCC (3.5 eq.) in THF at 20 °C for 4 days, achieved a conversion of 53%. Substituting DCC with PyBOP under identical conditions increased the end-group conversion for $\mathbf{A}^{R}$-$\mathbf{P_2}$-$\mathbf{E_3}$ (entry 2) to 60%. An improvement in the end-group conversion of 79% was observed for $\mathbf{A}^{R}$-$\mathbf{P_3}$-$\mathbf{E_3}$ (entry 3) upon changing the solvent from THF to DCM. The highest conversion of 92% was achieved for $\mathbf{A}^{R}$-$\mathbf{P_4}$-$\mathbf{E_3}$ (entry 4) by using Boc-Gly-OH (4.0 eq.), EDC (4.0 eq.) and DIPEA (10 eq.) in DCM. This superior performance is consistent with the formation of highly reactive *O*-acylisourea intermediates in EDC-mediated couplings, which effectively promotes amide bond formation in organic solvents like DCM, particularly in the presence of excess base that helps suppress side reactions and maintain nucleophilic activation.[31] A shorter reaction conducted in $CHCl_3$ at 50 °C for 1 day using EDC afforded a slightly reduced conversion for $\mathbf{A}^{S}$-$\mathbf{P_5}$-$\mathbf{E_3}$ (entry 5), at 69%, suggesting that an elevated temperature may partially compensate for the reduced reaction time. For FCA, end-group conversions remained low across the tested conditions. $\mathbf{A}^{R}$-$\mathbf{P_6}$-$\mathbf{E_4}$ (entry 6), synthesised with FCA (1.1 eq.), PyBOP (2.4 eq.) and DIPEA (6.0 eq.) in THF at 50 °C for 4 days, gave a conversion of 10%. Extending the reaction time to 10 days at 20 °C and increasing the FCA and PyBOP equivalents to 4.0 did not result in improved coupling efficiency for $\mathbf{A}^{S}$-$\mathbf{P_7}$-$\mathbf{E_4}$ (entry 7), which yielded only 24% conversion. These outcomes suggest that the low functionalization is not limited by stoichiometry but reflects the intrinsic limitations associated with the ferrocene unit. The combination of steric hindrance around the carboxyl group and the potential electronic effects likely reduces its effectiveness in promoting amide bond formation under the applied reaction conditions. Lipoic acid (both iLA and LA) consistently yielded the highest end-group conversions among all tested carboxylic acids, with values ranging from 62% to 97% depending on the reaction conditions. $\mathbf{A}^{R}$-$\mathbf{P_8}$-$\mathbf{E_1}$ (entry 8), prepared with iLA (1.0 eq.), PyBOP (1.2 eq.) and DIPEA (3.0 eq.), yielded a conversion of 62%. Increasing the reagent stoichiometry to 2.0 eq. of LA, 2.4 eq. of PyBOP, and 6 eq. of DIPEA enhanced the functionalization of $\mathbf{A}^{R}$-$\mathbf{P_{10}}$-$\mathbf{E_2}$ (entry 10) to 85%. An increase to 97% was observed for $\mathbf{A}^{R}$-$\mathbf{P_{11}}$-$\mathbf{E_2}$ (entry 11) at 50 °C under the same stoichiometry. An additional increase in the reagent equivalents of LA (4.0 eq.), PyBOP (4.8 eq.), and DIPEA (12.0 eq.) did not further improve the conversion of $\mathbf{A}^{R}$-$\mathbf{P_{12}}$-$\mathbf{E_2}$ (entry 12), suggesting a saturation point in reactivity. The high functionalization observed for lipoic acid may be attributed to a sterically accessible primary carboxyl group attached to a flexible aliphatic chain, which likely reduces conformational constraints and facilitates efficient approach of the coupling reagents to the polymer chain terminus under the applied heterogeneous conditions. For $\mathbf{B}^{R}$-$\mathbf{P_{13}}$-$\mathbf{E_1}$ (entry 13) and $\mathbf{B}^{S}$-$\mathbf{P_{14}}$-$\mathbf{E_1}$ (entry 14), performed in THF at room temperature with iLA (2.4 eq.), PyBOP (2.4 eq.) and DIPEA (6.0 eq.), a conversion of 83% was obtained. A similar high conversion was observed for $\mathbf{C}^{R}$-$\mathbf{P_{15}}$-$\mathbf{E_1}$ (82%) and $\mathbf{C}^{S}$-$\mathbf{P_{16}}$-$\mathbf{E_1}$ (85%) under identical reaction conditions. All corresponding MALDI-TOF MS spectra, including intensity data and simulated isotope patterns, are provided in the SI (see SI 24–54). Notably, lipoic acid demonstrated excellent reactivity for polymers initiated with both amine and alcohol initiators, underscoring its versatility as a coupling partner. The reproducibility of these outcomes across different initiator classes and stereochemical variants indicates that lipoic acid coupling proceeds with consistently high efficiency, providing a reliable route to gold-binding functionality. The unmodified parent polymers, designated $\mathbf{A}^{R}$-$\mathbf{P_0}$-$\mathbf{E_0}$, $\mathbf{B}^{R}$-$\mathbf{P_0}$-$\mathbf{E_0}$, and $\mathbf{C}^{R}$-$\mathbf{P_0}$-$\mathbf{E_0}$, served as references. Representative MALDI-TOF spectra of $\mathbf{A_0}$-$\mathbf{P_0}$-$\mathbf{E_0}$ and its functionalized derivatives – $\mathbf{A}^{R}$-$\mathbf{P_{10}}$-$\mathbf{E_2}$, $\mathbf{A}^{R}$-$\mathbf{P_4}$-$\mathbf{E_3}$ and $\mathbf{A}^{R}$-$\mathbf{P_6}$-$\mathbf{E_4}$ – are shown in Fig. 2(a–d). Comparison of spectra was used to assess end-group incorporation by monitoring shifts in peak positions corresponding to identical chain lengths and evaluating the relative intensities of the functionalized and parent peaks. In the case of $\mathbf{A}^{R}$-$\mathbf{P_{10}}$-$\mathbf{E_2}$ (Fig. 2b), the peak at m/z = 1633.934 corresponds to a sodium adduct of a poly(Aib) chain composed of 15 repeating units bearing the lipoic acid moiety

at the terminus. A minor peak at m/z = 1445.899 corresponds to the sodium adduct of the unmodified parent chain of the same length. The observed mass difference of 188 Da between the peaks corresponds to the replacement of the terminal hydrogen atom with the lipoic acid moiety, confirming successful incorporation of the end group. The peak at m/z = 1649.926 corresponds to the potassium adduct of the same functionalized chain, further validating the modification. In the case of $\mathbf{A^{R}\text{-}P_4\text{-}E_3}$ (Fig. 2c), the peak at m/z = 1603.114 corresponds to the sodium adduct of a poly(Aib) chain with 15 repeating units bearing the Boc-Gly unit at the chain terminus. In addition to the primary distribution, a second distribution of low-intensity peaks, highlighted in blue, is assigned to trace initiator-free chains arising from minor water-initiated or AMM-derived pathways, in which the amino terminus remains available for Boc-Gly coupling while the opposite C-terminus is hydroxyl terminated. Semi-quantitative comparison of the second series corresponds to 23% of the intensity of the main Boc-Gly-functionalized distribution for the same degree of polymerization. The observed mass shift of 157.09 between the functionalized and parent peaks corresponds to the replacement of the terminal hydrogen with the Boc-Gly unit, confirming successful incorporation of the end group. The subsequent removal of the Boc group was achieved in solution using TFA (1.1 eq.) in HFIP/H_2O (9 : 1, v/v), yielding poly(Aib) chains bearing a terminal glycine residue (see SI 38). In the case of $\mathbf{A^{R}\text{-}P_6\text{-}E_4}$ (Fig. 2d), the peak at m/z = 1557.000 corresponds to the lithium adduct of poly (Aib) with 15 repeating units. A minor sodium series corresponding to the ferrocene-functionalized chains was also observed. Notably, no unmodified lithium adduct was observed, suggesting selective ionization of the ferrocene-functionalized chains. Due to the absence of the unmodified chain in the lithium series, the percentage could not be determined from MALDI data. Additional analysis *via* ^{1}H NMR spectroscopy was employed to evaluate the end-group incorporation. Comparable analyses were carried out for the binaphthol-initiated $\mathbf{B^{R}\text{-}P_0\text{-}E_0}$ (Fig. 3a) and the Feringa overcrowded alkene photoswitch-initiated $\mathbf{C^{S}\text{-}P_0\text{-}E_0}$ (Fig. 3c) parent polymers and their iLA-functionalized derivatives. The peaks at m/z = 1840.106 for $\mathbf{B^{R}\text{-}P_0\text{-}E_0}$ and m/z = 1902.270 for $\mathbf{C^{S}\text{-}P_0\text{-}E_0}$ correspond to sodium adducts of poly(Aib) chains containing 18 repeating units, bearing the binaphthol and Feringa's photoswitch fragments, respectively, at the chain terminus. Upon coupling with iLA, new distributions were observed at m/z = 2028.162 for $\mathbf{B^{R}\text{-}P_{13}\text{-}E_1}$ (Fig. 3b) and m/z = 2090.173 for $\mathbf{C^{S}\text{-}P_{16}\text{-}E_1}$ (Fig. 3d), corresponding to the sodium adducts of the functionalized chains of identical length. The mass shift of 188 Da, relative to the parent peaks, is consistent with the replacement of the terminal hydrogen by the iLA moiety. The peaks at m/z = 1874.056 for $\mathbf{B^{R}\text{-}P_{13}\text{-}E_1}$ and m/z = 1936.064 for $\mathbf{C^{S}\text{-}P_{16}\text{-}E_1}$ correspond to the potassium adducts of the functionalized poly(Aib) chains with 16 repeating units, further corroborating the end-group assignments. The high relative intensity of these functionalized distributions relative to the corresponding parent distributions confirmed efficient incorporation of the iLA moiety at the polymer termini. MALDI-TOF spectra and simulated isotope patterns for all end-group functionalized derivatives listed in Table 1 are provided in the SI (SI 24–54).

Evaluation of chiral induction and helicity retention using circular dichroism (CD) spectroscopy

Circular Dichroism (CD) spectroscopy was employed to investigate chiral induction in poly(Aib) chains initiated from three distinct stereochemically different initiator classes (A*, B*, and C*) and to evaluate the retention of helicity upon end-group modification with isolipoic acid (E_1). As shown in Fig. 4a, all parent polymers (A*-, B*-, and C*-) exhibited distinct mirror-image spectra for the corresponding (*R*)- and (*S*)-enantiomeric initiators, confirming successful transfer of chiral information from the initiator to the otherwise achiral poly(Aib) backbone. $\mathbf{A^{S}\text{-}P_0\text{-}E_0}$ showed a strong positive band at 185 nm and a pronounced negative minimum at 220 nm, with additional weak shoulders near 200 nm and 210 nm. In contrast, $\mathbf{A^{R}\text{-}P_0\text{-}E_0}$ exhibited the exact inverse profile, with opposite signs at all the corresponding wavelengths. The observed features in the far-UV region are in agreement with literature reports for Aib-

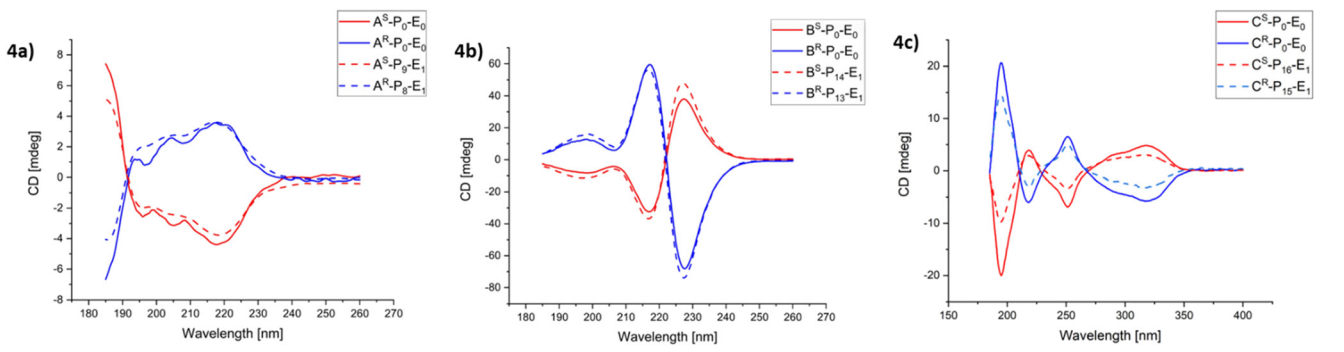

Fig. 4 Circular dichroism (CD) spectra of poly(Aib) chains initiated from (a) point-chiral amines (A*), (b) axially chiral binaphthols (B*), and (c) Feringa's photoswitches (C*), recorded in HFIP. Solid lines correspond to the unmodified parent polymers ($\mathbf{A^*/B^*/C^*\text{-}P_0\text{-}E_0}$) and the dashed lines to their isolipoic acid (E_1) functionalized derivatives.

containing peptides, where the π → π* transition is typically detected near 180 nm and n → π* transitions appear in the 190–230 nm range.[32] This overall spectral profile closely resembles the canonical signature of a 3_{10}-helix, which is characterised by a pronounced negative band near 220 nm arising from the peptide n → π* transition, together with a strong positive band around 190 nm from the π → π* transition.[33] Following the post-functionalization with isolipoic acid (E_1), the corresponding derivatives, $\mathbf{A^R\text{-}P_8\text{-}E_1}$ and $\mathbf{A^S\text{-}P_9\text{-}E_1}$, retained the characteristic mirror image profiles, demonstrating that attachment of the disulfide-containing end-group did not disrupt the helical secondary structure. The CD spectra of the binaphthol-initiated parent polymers, $\mathbf{B^R\text{-}P_0\text{-}E_0}$ and $\mathbf{B^S\text{-}P_0\text{-}E_0}$, showed distinct mirror-image profiles, confirming that the axial chirality of the initiator is effectively transferred to the poly(Aib) backbone. The absorption in the near-UV region indicates the influence of the binaphthol initiators. The pronounced chiral induction may be attributed to the rigid stereogenic axis of the binaphthol initiators, whose bulky and conformationally locked atropisomeric geometry is likely to impose a chiral bias at the chain terminus, thereby effectively directing the helical sense of the poly(Aib) backbone, as reported for related binaphthyl-based systems.[34] Following post-functionalization with isolipoic acid (E_1), the resulting derivatives $\mathbf{B^R\text{-}P_{13}\text{-}E_1}$ and $\mathbf{B^S\text{-}P_{14}\text{-}E_1}$ retained the mirror-image CD profiles, with comparable band positions and intensities to those of the unmodified parent polymers, demonstrating that the modification of the end-group did not compromise the secondary structure. The CD spectra of the photoswitch-initiated polymers $\mathbf{C^R\text{-}P_0\text{-}E_0}$ and $\mathbf{C^S\text{-}P_0\text{-}E_0}$ also revealed clear mirror-image profiles, demonstrating pronounced chiral induction from the photoswitch initiators. The twisted alkene-aryl framework of the photoswitch is inherently helically chiral, and such built-in helicity has been shown to bias the handedness of the supramolecular and polymeric assemblies.[35] Upon introduction of the isolipoic acid end-group (E_1), the photoswitch-initiated polymers $\mathbf{C^R\text{-}P_{15}\text{-}E_1}$ and $\mathbf{C^S\text{-}P_{16}\text{-}E_1}$ continued to display enantiomeric CD profiles, preserving the characteristic features of the parent chains. The incorporation of the disulfide-containing iLA unit provides an anchoring functionality for gold surfaces, and in combination with the inherent dynamic nature of the photoswitch scaffold, these systems present the potential for creating responsive, surface-bound chiral architectures in which the helicity, in principle, can be reversibly switched. Chiral polymer architectures at interfaces also provide opportunities to access a range of effects arising from molecular chirality, including spin-dependent and charge transport phenomena.[36] The CD spectra of the additional point-chiral derivatives, $\mathbf{A^R\text{-}P_4\text{-}E_3}$ and $\mathbf{A^S\text{-}P_3\text{-}E_3}$ (Boc-Gly-OH functionalized), $\mathbf{A^R\text{-}P_6\text{-}E_4}$ and $\mathbf{A^S\text{-}P_7\text{-}E_4}$ (FCA functionalized), are provided in the SI (see SI 56 and 57). To further probe the induced chiral environment suggested by the CD spectra, the terminal Boc-Gly unit was explored as a local ^{1}H NMR reporter, analogous to reporter-group approaches used in Aib foldamers.[37] Although partial splitting of the glycine CH_2 resonance was observed (see SI 19), the chemical-shift differences were not sufficiently well resolved for a quantitative determination of helicity excess in the present polymeric system. Additional secondary-structure estimation using CD Multivariate SSE (JASCO Spectra Manager™) analysis was carried out for the point-chiral and binaphthol initiated systems, and the estimated helical content values from the secondary structure were determined and are provided in the SI (SI 62 and SI Table 2). The corresponding analysis was not performed for the Feringa-photoswitch initiated polymers, as the available software models were not applicable to the spectral range of these systems. No significant changes in the estimated helical content were observed after the modification, consistent with retention of the overall helical secondary structure.

End-group mediated anchoring of poly(Aib) chains to gold surfaces: AFM and XPS analysis

To evaluate the ability of end-group functionalized poly(Aib) chains to adhere to gold surfaces *via* disulfide–gold interactions, atomic force microscopy (AFM) was employed. Specifically, polymers bearing terminal lipoic acid moieties ($\mathbf{A^S\text{-}P_9\text{-}E_1}$) were adsorbed onto a gold substrate by immersing the substrate in a 2 mg ml^{-1} solution of the polymer in HFIP for 24 hours, to form layers *via* thiol–gold affinity. The overall flow scheme of the coating process is provided in the SI (see SI 61). AFM topography analysis revealed a marked increase in surface roughness (in the highlighted area) upon polymer deposition. As shown in Fig. 5a and b, the bare gold substrate exhibited a root-mean-square (RMS) roughness of 0.240 nm, while surfaces treated with the isolipoic acid-terminated polymer displayed an RMS roughness of 1.607 nm. This increase is indicative of surface coverage by the polymer film and is consistent with the formation of a surface-bound layer driven by disulfide–gold binding. To further investigate the film morphology, selective etching of the gold substrate was performed using dilute HCl, allowing for the estimation of the polymer height from the resulting edge profile. The height difference across the etched boundary corresponds to ~15–20 nm, supporting the formation of a polymer film on the gold substrate (see SI 58). To complement the AFM analysis, X-ray photoelectron spectroscopy (XPS) was performed to probe the surface composition of the polymer-functionalized gold substrates. As shown in Fig. 5d, the gold substrate treated with lipoic acid-terminated poly(Aib) ($\mathbf{A^S\text{-}P_9\text{-}E_1}$) revealed a distinct N peak centred at ~400 eV, characteristic of the amide nitrogen within the polypeptide backbone. Additional evidence for the surface anchoring is provided by the S 2p region, which exhibits a sulphur signal at 163–164 eV (see SI 59), corresponding to the sulphur species derived from the lipoic acid anchoring group interacting with the gold surface. Together, these complementary techniques confirm the successful immobilization of the poly(Aib) chains *via* the isolipoic acid end-group, establishing a strategy for anchoring helical polypeptides onto the gold interfaces.

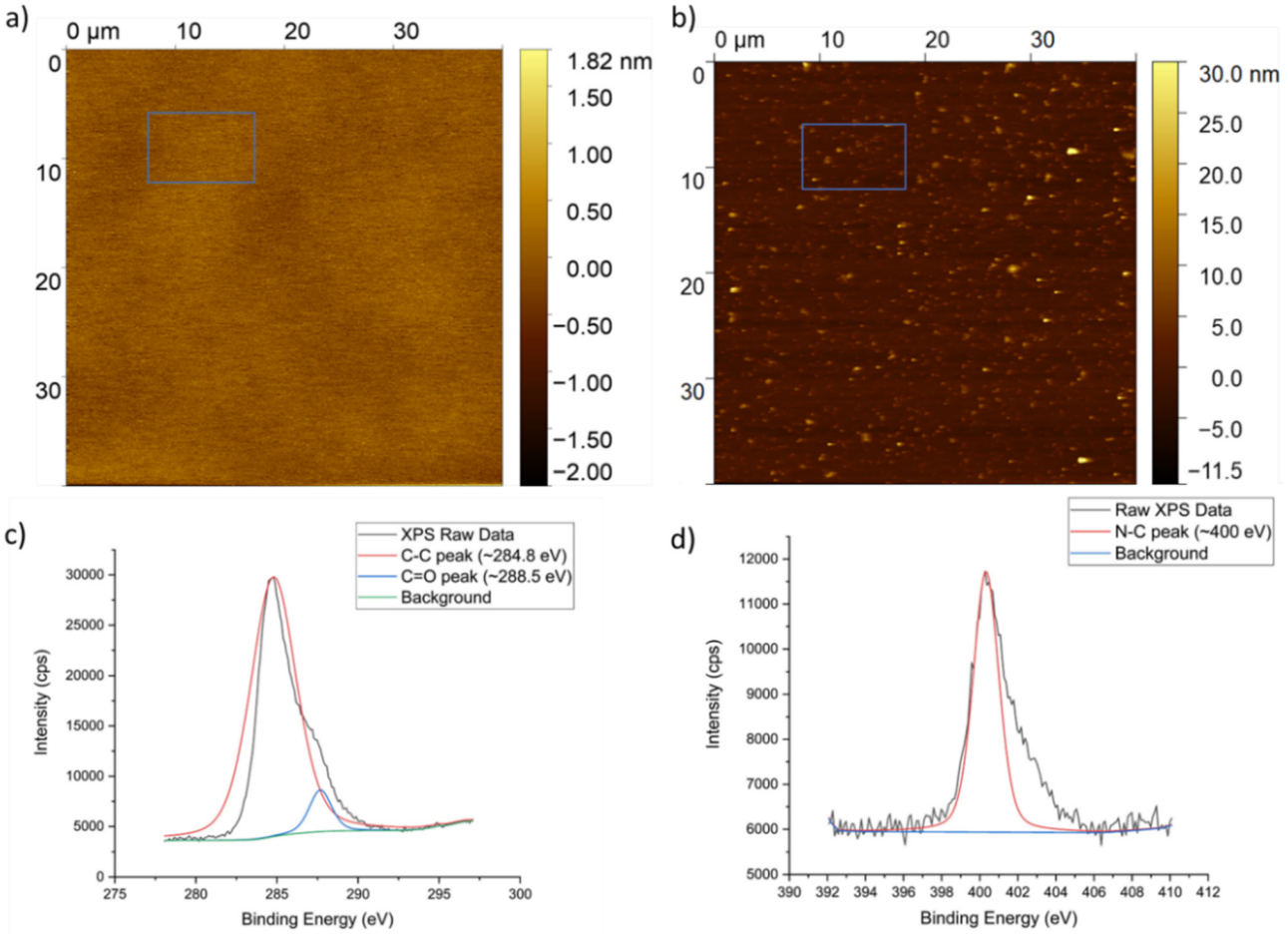

Fig. 5 (a) AFM topography of the bare gold substrate, (b) AFM topography of the gold substrate after adsorption of the lipoic-acid terminated polymer (A^S-P_9-E_1), (c) XPS C 1s spectrum of the polymer-functionalized gold surface showing characteristic contributions from C–C (~284.8 eV) and C═O (~288.5 eV) functionalities, consistent with the presence of the polymer backbone and the terminal groups, and (d) XPS N 1s spectrum of the polymer functionalized gold surface, displaying a characteristic N–C peak at (~400 eV), indicative of the nitrogen present in the polymer backbone (A^S-P_9-E_1).

Conclusion

In this work, we have demonstrated a robust approach for the post-functionalization of poly(Aib) chains directly after NCA ring-opening polymerization, under heterogeneous conditions. We aim to generate perfectly endgroup-modified polymers, where different chiral head groups (point-chiral, axial-chiral, photoswitchable) are combined with a poly(AiB) chain of defined length, and a nonchiral endgroup, able to bind to Au-surfaces for further studying the chiral induced spin selectivity effect (CISS). By employing stereochemically diverse initiators – point chiral amines, axially chiral binaphthols, and Feringa-type overcrowded alkene-based photoswitches – we achieved a clear induction of a preferred helical sense into the otherwise achiral poly(Aib) backbone, as confirmed by CD spectroscopy. Subsequent end-group functionalization with isolipoic acid, α-lipoic acid, Boc-Gly-OH, and ferrocene carboxylic acid was successfully carried out under optimised peptide-coupling conditions, with conversions ranging from modest to nearly quantitative, depending on the steric and electronic properties of the end group. MALDI-TOF mass spectroscopy provided evidence of end-group modification, while CD spectra confirmed that the helical secondary structure was retained after modification. Among the tested end groups, lipoic acid derivatives proved particularly effective, yielding consistently high conversion across all initiator classes and providing a versatile disulfide handle for surface attachment. AFM and XPS results indicated that the lipoic acid-terminated helices can adsorb onto the gold surfaces, forming surface-bound polymer layers. Overall, this study highlights the utility of stereochemically diverse initiators combined with post-polymerisation functionalization to generate a broad family of helical poly(Aib) derivatives. Importantly, by integrating static and dynamic initiators with surface-anchored end groups, this strategy offers the potential to create dynamic, switchable chiral interfaces, in which molecular-level helicity can be harnessed to generate responsive surface architectures for exciting spintronics.

Author contributions

S. R., C. H., and M. R. conducted the synthesis and characterization of the polymers. Y. X. conducted XPS measurements. J. D. grew the gold substrate. J. F. T. conducted the AFM experiments. S. R. and W. H. B. wrote the manuscript. W. H. B. is the corresponding author, who planned the research, secured funding, and corrected the manuscript.

Conflicts of interest

There are no conflicts to declare.

Data availability

The data that support the findings of this study are available from the corresponding author upon reasonable request. All original data are stored in electronic lab notebooks and are thus available upon request. The data supporting the findings of this study are provided in the supporting information. These include synthetic procedures, NMR spectra, MALDI-TOF MS spectra and simulations, Circular Dichroism (CD) spectra, XPS and AFM data.

Supplementary information (SI) is available. See DOI: https://doi.org/10.1039/d6py00149a.

Acknowledgements

W. H. B., S. R., C. H., and M. R. acknowledge funding from the grants DFG 1337/17-1 (542011057); 1337/16-1 (506699569) and 1337/18-1 (551070679); INST 271-441/FUG (524610847) and the excellence cluster initiative PoliFaces. W. H. B. further acknowledges the DFG-cluster of excellence, the Center for Chiral Electronics, EXC 3112/1-533767171 (Center for Chiral Electronics) and the Max Planck Research School (IMPRS) for their support.

References

1 M. Rohmer, J. Freudenberg and W. H. Binder, *Macromol. Biosci.*, 2023, **23**, 2200344.
2 C. Adam, A. D. Peters, M. G. Lizio, G. F. S. Whitehead, V. Diemer, J. A. Cooper, S. L. Cockroft, J. Clayden and S. J. Webb, *Chem. – Eur. J.*, 2018, **24**, 2249–2256.
3 S. J. Pike, J. E. Jones, J. Raftery, J. Clayden and S. J. Webb, *Org. Biomol. Chem.*, 2015, **13**, 9580–9584.
4 S. J. Pike, V. Diemer, J. Raftery, S. J. Webb and J. Clayden, *Chem. – Eur. J.*, 2014, **20**, 15981–15990.
5 S. Aravinda, N. Shamala and P. Balaram, *Chem. Biodiversity*, 2008, **5**, 1238–1262.
6 C. Toniolo and E. Benedetti, *Trends Biochem. Sci.*, 1991, **16**, 350–353.
7 B. Di Blasio, A. Santini, V. Pavone, C. Pedone, E. Benedetti, V. Moretto, M. Crisma and C. Toniolo, *Struct. Chem.*, 1991, **2**, 523–527.
8 I. L. Karle and P. Balaram, *Biochemistry*, 1990, **i9**, 6747–6756.
9 R. P. Hummel, C. Toniolo and G. Jung, *Angew. Chem., Int. Ed. Engl.*, 1987, **26**, 1150–1152.
10 T. Leigh and P. Fernández-Trillo, *Nat. Rev. Chem.*, 2020, **4**, 291–310.
11 P. Kumar, N. G. Paterson, J. Clayden and D. N. Woolfson, *Nature*, 2022, **607**, 387–392.
12 M. Pollastrini, G. Marafon, J. Clayden and A. Moretto, *Chem. Commun.*, 2021, **57**, 2269–2272.
13 D. Mazzier, M. Crisma, M. De Poli, G. Marafon, C. Peggion and J. Clayden, *J. Am. Chem. Soc.*, 2016, **138**, 8007–8018.
14 B. A. F. Le Bailly and J. Clayden, *Chem. Commun.*, 2016, **52**, 4852–4863.
15 S. M. Morrow, A. J. Bissette and S. P. Fletcher, *Nat. Nanotechnol.*, 2017, **12**, 410–419.
16 J. Freudenberg and W. H. Binder, Chirality Control of Screw-Sense in Aib-Polymers, *ACS Macro Lett.*, 2020, 686–692.
17 M. Rohmer, S. G. Ebbinghaus, K. Busse, J. Radicke, J. Kressler and W. H. Binder, *Chem. Eur. J.*, 2023, **29**, e202302585.
18 M. Rohmer, Ö. Ucak, R. Fredrick and W. H. Binder, *Polym. Chem.*, 2021, **12**, 6252–6262.
19 O. Nuyken and S. Pask, *Polymers*, 2013, **5**, 361–403.
20 N. Hadjichristidis, H. Latrou, M. Pitsikalis and G. Sakellariou, *Chem. Rev.*, 2009, **109**, 5528–5578.
21 D. Huesmann, K. Klinker and M. Barz, *Polym. Chem.*, 2017, **8**(6), 957–971.
22 Y. Li, R. Chang and Y. X. Chen, *Chem. – Asian J.*, 2022, **17**(14), e202200318.
23 Y. Xia, Z. Song, Z. Tan, T. Xue, S. Wei, L. Zhu, Y. Yang, H. Fu and Y. Jiang, *Nat. Commun.*, 2021, **12**(1), 732.
24 T. J. Deming, *Synthesis and Self-Assembly of Well-Defined Block Copolypeptides via Controlled NCA Polymerization*, Springer International Publishing, 2013, pp. 1–37.
25 W. Agut, R. Agnaou, S. Lecommandoux and D. Taton, *Macromol. Rapid Commun.*, 2008, **29**(12–13), 1147–1155.
26 D. Leboeuf, *Trends Chem.*, 2025, **7**(5), 205–207.
27 J. Freudenberg and W. H. Binder, *ACS Macro Lett.*, 2020, **9**, 686–692.
28 T. Van Leeuwen, J. Gan, J. C. M. Kistemaker, S. F. Pizzolato, M. C. Chang and B. L. Feringa, *Chem. – Eur. J.*, 2016, **22**, 7054–7058.
29 A. El-Faham and F. Albericio, *Chem. Rev.*, 2011, **111**, 6557–6602.
30 H. Chen, M. He, J. Pei and H. He, *Anal. Chem.*, 2003, **75**(23), 6531–6535.
31 W. H. Binder, B. Pulamagatta, O. Kir, S. Kurzhals, H. Barqawi and S. Tanner, *Macromolecules*, 2009, **42**, 9457–9466.
32 K. A. Bode and J. Applequist, *J. Phys. Chem.*, 1996, **100**, 17825–17834.

33 A. Moretto, F. Formaggio, B. Kaptein, Q. B. Broxterman, L. Wu, T. A. Keiderling and C. Toniolo, *Biopolymers*, 2008, **90**, 567–574.
34 E. Yashima, *Proc. Jpn. Acad. Ser. B*, 2023, **99**, 438–459.
35 B. L. Feringa, *Angew. Chem., Int. Ed.*, 2017, **56**, 11060–11078.
36 M. Rohmer, Y. Xie, S. Roy, C. Hildebrand, J. F. Thümmler, J. Deka, P. K. Sivakumar, S. S. P. Parkin, T. N. H. Nguyen, L. T. Baczewski, C. Tegenkamp and W. H. Binder, *Commun. Mater.*, 2026, **7**, 46.
37 B. A. F. Le Bailly, L. Byrne, V. Diemer, M. Foroozandeh, G. A. Morris and J. Clayden, *Chem. Sci.*, 2015, **6**(4), 2313–2322.